Use of Resonant Acoustic Fields as Atmospheric-Pressure Ion Gates

Julia L. Danischewski[1], Yi You[2], Lauren S. Bauer[1], Jens Riedel[2], Jacob T. Shelley[1*]

[1] Department of Chemistry and Chemical Biology, Rensselaer Polytechnic Institute, Troy, NY 12180, USA

[2]Bundesanstalt für Materialforschung und -prüfung (BAM), Berlin 12489 Germany

* Corresponding author: Jacob T. Shelley, E-mail: shellj@rpi.edu

ABSTRACT

Ion optics are crucial for spectrometric methods such as mass spectrometry (MS) and ion mobility spectrometry (IMS). Among the wide selection of ion optics, temporal ion gates are of particular importance for time-of-flight MS (TOF-MS) and drift-tube IMS. Commonly implemented as electrostatic ion gates, these optics offer a rapid, efficient means to block ion beams and form discrete ion packets for subsequent analysis. Unfortunately, these devices rely on pulsed high-voltage sources and are not fully transparent, even in their open state, which can lead to ion losses and contamination. Here, a novel atmospheric-pressure ion gate based on a resonant acoustic field structure is described. This effect was accomplished through the formation of a resonant, standing acoustic wave of alternating nodes and antinodes. Alignment of an atmospheric-pressure gaseous ion beam with an antinode, *i.e.* a region of transient pressure, of the acoustic structure acted as a gate and blocked ions from impinging ion-selective detectors, such as a mass spectrometer and a Faraday plate. The velocity of the ion stream and acoustic power were found to be critical parameters for gating efficiency. In the presence of an acoustic field (i.e. a closed gate), ion signals were decreased by as much as 99.8% with a response time faster than the readout of the ion-measurement devices used here (*ca.* 75 ms). This work demonstrates the basis for a low-cost, acoustic ion gate, which is optically transparent and easily constructed with low-power, off-the-shelf components, that can be used in MS and IMS instrumentation.

INTRODUCTION

Ion-based spectrometries are an invaluable resource for accurate, sensitive, and selective chemical analysis. Techniques such as mass spectrometry (MS) and ion mobility spectrometry (IMS) use so-called ion optics to shape the observed ions trajectories on the desired path. Analogous to light optics, the individual components are used to focus, block, separate, and guide ion beams.[1] Ion gates, also referred to as ion shutters, are a particularly important type of ion optic because they control the flow of ions. When the gate is open, ions can proceed into a designated region, and when the gate is closed, they are blocked. Pulsed ion spectrometries, such as time-of-flight (TOF) MS and drift tube (DT) IMS, rely on these gates to form discrete ion packets for mass-to-charge and collision cross section measurements.[3,4] As such, electrostatic ion gates must operate in a variety of pressure regimes, from atmospheric pressure to high vacuum, to meet the diverse requirements of the surrounding instrument.[5] The opening and closing of the gate divides the ions into discrete ion packets, which are advanced into the analysis region by applying an injection pulse when the gate is open. The formation of ion packets and controlled release of ions from the gate region ultimately dictate the resolution and sensitivity.[5] Separation and uniformity of ion packets helps to minimize peak broadening for time-dispersive techniques such as TOF-MS and DT-IMS.[2,5,6] Other instruments, such as linear ion traps (LITs) use gates in the form of endcap electrodes to ensure that ions remain in storage sufficiently long to be collisionally cooled, collisionally activated for dissociation, or undergo other ion-molecular interactions, prior to mass analysis.[7]

Bradbury-Nielsen gates (BNGs) are commonly used in IMS instrumentation due to their ability to open and close within nanoseconds.[8–10] This gate is formed from coplanar, interdigitated wires, where adjacent wires are biased with alternating polarities relative to a reference potential (*cf.* **SI1**).[5,10] Spacing of the wires ranges from 50 μm to more than 1 mm depending on the application.[11] Wire diameter also varies from tens to hundreds of micrometers.[11] The combined diameter and wire spacing dictate the transmission and efficacy of the gate, as the interplay of these two factors will influence the resulting cross section covered by wires as well as the formed electric field. For the gate to transmit (*i.e.* gate is open), the wires are placed at the same potential. The gate is closed when opposite polarity electric potentials are applied to adjacent

wires, which establishes a strong electric field barrier larger than the ion beam's momentum and causes the ions to deviate from their initial path.[5,9,10,12] While changes of tens of volts on the BNG are sufficient to cause ion deflection and gating, it is common to reference the gate to the drift voltage of the IMS, typically at kilovolt potentials.[11,13] Furthermore, the interaction between the BNG field and drift field behind the gate leads to the formation of a depletion region, where ions that have not traveled far enough past the gate will be pulled back towards the gate and neutralized.[5] Recent work has also shown that a depletion region exists on the ionization side of the gate, due to the penetration of the closing field of the BNG into the ionization region.[14] Additionally, ions collide with the gate wires, which causes neutralization that leads to poorer sensitivity and contamination.[11–13] Depending on the arrangement, in common instruments about 2 % to 20 % of the gate cross section is covered by wires.[11] Although decreased wire spacing can lead to benefits such as smaller applied voltages and faster modulation times, but with a sacrifice in optical transparency.[11] Maintenance and adaptation to different sizes and environments becomes challenging for BNGs, as it may disrupt the wire spacing or break wires and lead to changes in the efficacy of the shutter by introducing non-idealities in the electric fields.[5,13] Wire placement must be within 10-µm tolerance, as imprecision in position leads to inconsistent deflection of ions and a less effective gate for wire spacings of less than 75 µm.[11]

The Tyndall-Powell ion gate (TPG) relies on a similar principle of pulsed electrostatic fields to deflect ions. However, a TPG consists of two wire grids spaced apart by *ca.* 1 mm in the direction of the ion beam and held at opposite potentials (*cf.* **SI1**).[14] The sequence of grid potentials used depends on the polarity of ions to be gated.[15] For positive ion gating, the first and second grids are negatively and positively charged, respectively, when the gate is closed. To open the gate, the polarity is reversed.[15] While TPGs are simpler to construct and easier to maintain, there are several drawbacks. The presence of two meshes leads to the formation of a larger, well-defined depletion region between the screens,[9] and there is more surface area for ion losses and contamination.[5,9,13,16] Additionally, the wider fill region of the TPG increases the time needed for the ions to traverse the gate when open, which is typically on the order of milliseconds, resulting in

wider ion packets.[5,14,16,17] Changes to the gating potentials and timing of the fields can alleviate these challenges and improve TPG transmission to near ideal, but require custom-built electronics and pulsed high voltages (*e.g.*, 5 kV) to be implemented.[16,18]

A more idealized ion gate would be one that is easy to construct and maintain, as well as minimize analyte-ion loss and contamination. One possibility for such an ion gate draws on a recently discovered form of ion manipulation that is not based on external electric or magnetic fields, but instead utilizes acoustic fields to redirect, focus, and deflect ions at atmospheric pressure.[19] This acoustic ion manipulation (AIM) phenomenon was initially shown through the interaction of a gaseous ion beam with a resonant, standing acoustic field structure.[19] The field can be formed through the interference of two opposing longitudinal wavefronts of equal frequency and amplitude.[20–23] Along the propagation direction of the sound, alternating areas of stable and unstable pressure, referred to as nodes and antinodes, respectively, are formed. Nodes repeat every $\frac{\lambda}{2}$, where λ is the wavelength of sound in the propagation medium, while antinodes are located in the space between nodes.[20–22] When an ion beam is orthogonal to the resonant acoustic field, gaseous ions preferentially pass through nodal regions, and are repelled from time-varying pressures in the antinodes.[19] Because there are no physical obstructions in the ion beam path ion transmission with AIM should be better than electrostatic gates. Here, we characterize the critical parameters for the control of ion transmission through an AIM ion gate with both MS and Faraday-plate detectors.

EXPERIMENTAL SECTION

Ionization source. A pin-to-capillary flowing atmospheric-pressure afterglow (FAPA) ionization source was used to generate a partially ionized beam of gas.[24] The exact source design used here has been described in detail elsewhere.[24–26] Briefly, an atmospheric-pressure glow discharge was maintained between a pin cathode and tube-shaped anode in a gastight chamber. The plasma was operated with a discharge current between 5 and 15 mA with a custom-built high-voltage power supply (Prosolia, Inc. Indianapolis, IN) and

sustained in an ultra-high purity helium support gas (99.999% pure, AirGas, Radnor, PA) with a flow rate between 0.5 and 1.5 L min^{-1} (model C50L-AL-DD-2-PV2-V0-SCR, Sierra Instruments, Monterey, CA). Gas flow from the source outlet was laminar and supported the mass transport of the ions to the detector.[27,28] In some cases, the exit capillary of the FAPA was biased between 0 and 100 V with a DC-power supply (model 230-01F, Spellman, Valhalla, NY) to bias the polarity of ions exiting the source. For some experiments, the ion beam was doped with aniline (99.5% purity, Millipore Sigma, Burlington, MA) by flowing ultra-high purity nitrogen gas (99.999% pure, AirGas, Radnor, PA) over a small aliquot of liquid aniline in a vial. Two fused-silica capillaries (101.0 µm i.d., 360.0 µm o.d., Polymicro Technologies, Phoenix, AZ) were punched through the septum of the vial to serve as an inlet and an outlet. Nitrogen gas flow was regulated with a mass flow controller (GR116-06, Fathom Technologies, Georgetown, TX) and was typically 0.06 L min^{-1}. The outlet capillary from the vial was positioned between the exit of the FAPA source and the acoustic resonator (*cf.* **SI2**).

Standing acoustic wave ion gate. A standing acoustic wave was formed with two opposing ultrasonic piezoelectric speakers (TCT40-16R/T, HiLetgo, Guangdong, China) spaced 16 mm apart. Each transducer was driven with a 20 V_{p-p} sine wave (unless otherwise noted) from an arbitrary waveform generator (model AG2052F, Owon Technology Inc., Zhangzhou, China), 180° out of phase with one another at their resonant frequency of 37.8 kHz. The resonant frequency was determined with an LCR meter (B&K Precision 891, B&K Precision Corporation, Yorba Linda, California). Since the speakers were driven out-of-phase, the total applied voltage was 40 V_{p-p} between the two opposing surfaces of the transducers. It is important to note that the cases that surrounded the speakers were electrically grounded, thus no electric field was present in the standing-wave region. Standing-wave formation was confirmed with an oscilloscope (InfiniiVision DSQ-X 2024A, Keysight Technologies Inc., Santa Rosa, CA), driving one speaker as a transmitter, while the other was connected to the oscilloscope and acted as a receiver. Under ideal resonance conditions, standing-wave formation was achieved at the speaker distance corresponding to maximum output voltage from the receiver.

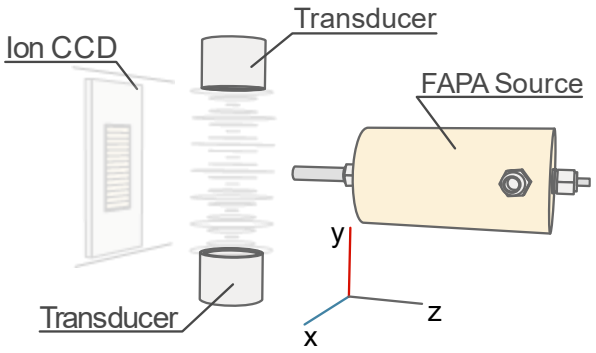

Figure 1: A schematic of the experimental set-up, with the IonCCD as a detector. The vertical alignment of the IonCCD shown here has the array oriented along the y-axis. The IonCCD was horizontally aligned when positioned along the x-axis.

Ion detection methods. Three different detection methods were used to record ion-beam behavior. A Faraday plate with a picoammeter (model 51097A, Keithley Instruments Inc., Cleveland, OH) provided bulk ion-current measurements without the influence of a vacuum region. An insulating mask with a 7-mm^2 round hole was placed over the Faraday plate to limit the detection area. Ion beam position and signal were monitored with an IonCCD detector array (IDS-2030, OI Analytical/CMS Field Products, Pelham, AL). The 1D-array detector consisted of 2126 pixels, each 21 µm by 1500 µm with ~88% pixel area ratio,[29] and was oriented in different directions to observe ion profiles. In vertical alignment, the array was oriented in the same direction as the longitudinal acoustic wave propagation, while in horizontal alignment the IonCCD was orthogonal to the acoustic-field structure (*cf.* **Figure 1**). A Q-Exactive mass spectrometer (Thermo Scientific, Bremen, Germany) was used to detect ions when the AIM gate was located directly before the inlet to the vacuum environment of the MS. The maximum ion injection time and mass resolving power were set to 200 ms and 70,000, respectively. The mass range was *m/z* 50 to *m/z* 200 to record lower-mass ions produced from the FAPA source. During gate operation, the ionization source and detector were separated by *ca.* 16 mm to accommodate the width of transducers used for standing-wave formation.

SAFETY CONSIDERATIONS. Hazardous exposed DC voltages were present on the FAPA, and care was taken to avoid contact with charged surfaces. Other personal protective equipment, such as gloves and safety goggles, were used as necessary for each experiment. While the transducers may reach *ca.* 120 dB at a driving voltage of 20 $V_{p\text{-}p}$, no hearing protection was necessary as the sound is highly directional with a *ca.* 60° cone angle (-6 dB) in the orientation of the transducer.[30] In addition, the frequency of ultrasound used here (*ca.* 40 kHz) is not considered hazardous for human hearing.

RESULTS AND DISCUSSION

Much of the underlying theory behind AIM is still in development, due to the recent nature of its discovery.[19] Previous work has demonstrated the broad capabilities of AIM, including deflection, focusing, gating, and separation.[19] Gating is of particular interest, as acoustic ion gates can efficiently block ions using inexpensive and robust components. However, the impact of different acoustic field properties or instrumental parameters on the efficacy of acoustic ion gates has not been detailed yet. As such, it was important to validate acoustic-ion interactions with a variety of detectors to account for instrument effects (*e.g.*, vacuum pull and external electric fields) and develop optimized operational conditions for a variety of detection methods. Initially, AIM gating was observed with Faraday plate detectors, as they can be operated at atmospheric pressure and do not require additional electric fields. The FAPA source generated atmospheric reagent ions that were sufficient for observing the interactions of a partially charged ion beam with the acoustic gate. The support gas flow rate was selected to ensure efficient transport of ions from the source to the detector, while the discharge current was kept low to prevent possible photon-induced signals from the IonCCD detector used in accompanying experiments.[31] Additionally, the presence of an electrical bias on the FAPA source outlet had multiple benefits for the experiment, including a potential difference that drove ions towards the lower potential (*i.e.* the detector), and enhanced unipolarity of the ion beam towards positive ions.[24,26]

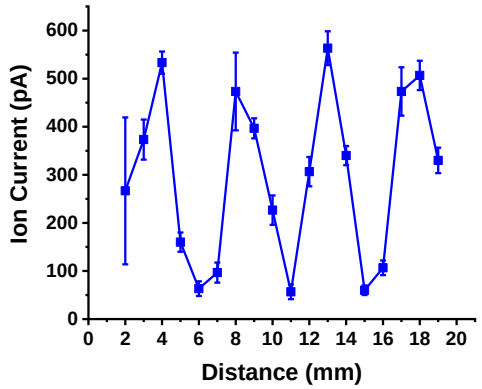

Figure 2: Faraday plate ion current as a function of vertical position relative to the acosutic resonator. The FAPA outlet (center) was aligned with the bottom speaker at a height of 0 mm. FAPA source conditions were 0.75 L min^{-1} He flow, 3-mA discharge current, and +50 V applied to the source outlet. The speakers were driven with sine waves at 37.8 kHz, 40 $V_{p\text{-}p}$.

A profile of ion response to the acoustic field was generated by recording the ion signal at different points of height in the standing acoustic wave (y in **Figure 1**). The acoustic field was scanned between the FAPA source and masked Faraday plate, so that different pressure regions were present in the ion beam path. A sinusoidal pattern was observed (*cf.* **Figure 2**), where maxima occurred approximately 4 mm apart, as did the ion-signal minima. This spacing reflected the expected distance between nodes and antinodes for the given transducer frequency (37.8 kHz) in air, based on a theoretical wavelength calculated for a speed-of-sound of *ca.* 340 ms^{-1}.[19–22] Previous work has demonstrated that the presence of an antinode in the ion beam path shifts the ion beam by roughly $\frac{\lambda}{4}$ along the axis of acoustic-field propagation, or half the distance between antinodes.[19] Here, the ion signal declines by more than 85% when aligned with the acoustic antinode under these conditions. It is important to note that the presence of multiple antinodes in the resonant acoustic structure offers several locations that could be used for gating. The antinode in the center of the standing acoustic wave was selected as the gate for subsequent experiments described here, to minimize the chance of the speakers being in the path of the ion beam after deflection.

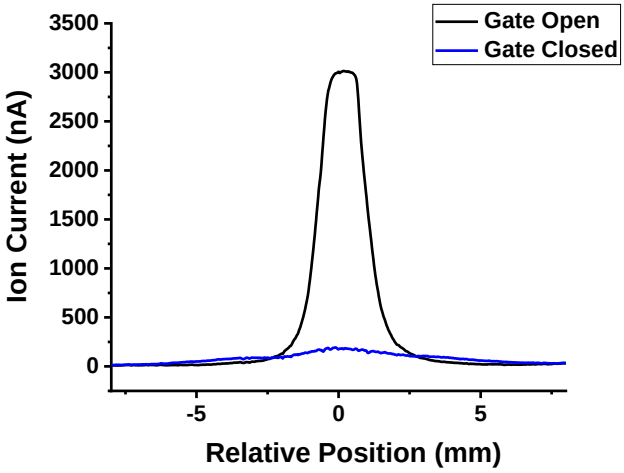

Figure 3: Ion beam position with and without an acoustic gate as determined by an IonCCD, which was oriented perpendicular to the direction of acoustic field propagation. FAPA source conditions were the same as in figure 2. The acoustic field was driven with sine waves at 37.8 kHz, 40 $V_{p\text{-}p}$.

In the next experiment, the IonCCD was aligned perpendicular to the acoustic field structure (*i.e.* "horizontal" alignment) to assess ion gating with the central acoustic antinode (*cf.* **Figure 3**). In this configuration, the total summed ion signal decreased by 88%, without any observed horizontal shift to the beam position. The decline in signal was attributed to deflection of the ion beam above or below the detector pixels. While the ion beam was *ca.* 3 mm in diameter based on the carrier gas beam width,[27] the distance between nodes and antinodes is 2 mm and covers the 1.5-mm tall pixels of the IonCCD. However, some signal was still observed on the IonCCD after deflection, indicating that some ions may be able to pass through the antinode region. This detector orientation is most comparable to alternate detectors, such as the Faraday collector and MS, where the gate function also depends on the deflection of ions outside of an acceptance region.

As ion gates are an important optic for both vacuum and higher-pressure ion spectroscopy instrumentation, direct comparisons of gate function with Faraday plate, IonCCD, and mass-spectrometric detection were made. The ionization source parameters were kept constant across experiments to study the impact of different instrumental features (*e.g.*, vacuum and external electric fields). It is important to note

that transmission through the open gate was defined as 100%, as there was no physical obstruction in the ion beam path, unlike electrostatic gates (*cf.* **SI 3**). Closed-gate transmission was calculated as shown in **Equation 1**

$$\%T = 100 * \frac{I}{I_0} \quad (1)$$

where %T is the transmission, I_0 is the signal when the gate is open, and I is the signal when the gate is closed. Error is the standard deviation of three calculated transmissions. Here, transmission signifies that ions are unintentionally passing through the closed gate. As such, it is considered analogous to leakage and the two terms are used interchangeably. For Figure 2B, transmission was calculated to be 13.2 ± 0.5% from the integrated ion current when the IonCCD was horizontal with respect to acoustic field propagation. For the Faraday collector and mass spectrometer, transmission was calculated based on ion current or reconstructed total ion current (RTIC), respectively. Transmission through an antinode was 18.2 ± 2.0% and 66.5±2.8% with the Faraday collector and mass spectrometer as the detector, respectively (*cf.* **Figure 4**).

Although the same source conditions were used, the leakage of ions through the closed gate varied significantly. Minor differences in leakage between the IonCCD and Faraday collector can be attributed to differences in detector cross section. Much greater ion leakage was observed with the mass spectrometer, however, possibly due to instrumental effects. The pull of the vacuum environment of the mass spectrometer through the atmospheric-pressure interface produces a negative pressure region and offers an additional force to pull the ions towards the MS inlet through the antinode. Simulations and experiments have shown that the flow rate of gas into an MS inlet capillary is between 1.5 and 2 L min^{-1} for a 58.5-mm tube with 0.58 mm i.d. and differential pressure of *ca.* 1000 mbar, which is similar to the inlet of the Q-Exactive used here.[32]

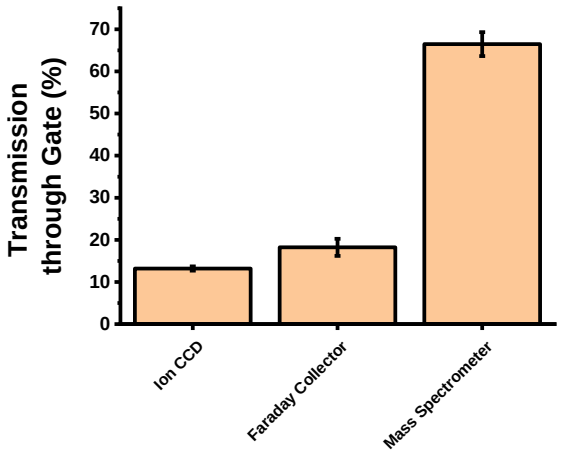

Figure 4: Comparison of ion transmission through a closed gate operated at 40 $V_{p\text{-}p}$ for the IonCCD, Faraday collector, and MS detectors with the same source conditions (He flow rate: 0.75 L min^{-1}, discharge current: 3 mA, front plate bias: 50V), and acoustic field conditions (37.8 kHz).

The impact of instrumental features on acoustic ion gating is clear, however it is also important to understand the role of acoustic power in AIM deflection. The degree of ion blockage from a mass spectrometer was determined as a function of applied voltage to the transducer array and acoustic power. At low applied amplitudes, between 0 and 20 $V_{p\text{-}p}$, little loss in ion signal was observed (*cf.* **Figure 5a**). At 30 $V_{p\text{-}p}$, however, ion signal decreased by *ca.* 50%, and then almost completely blocked at 40 $V_{p\text{-}p}$. More interesting, however, was the relation between the acoustic power and transmission through the antinode. The acoustic power is related to the driving voltage of a transducer as shown in **Equation 2**[30]

$$P_{\text{acoustic}} \propto \frac{{V_{\text{peak}}}^2}{R} \tag{2}$$

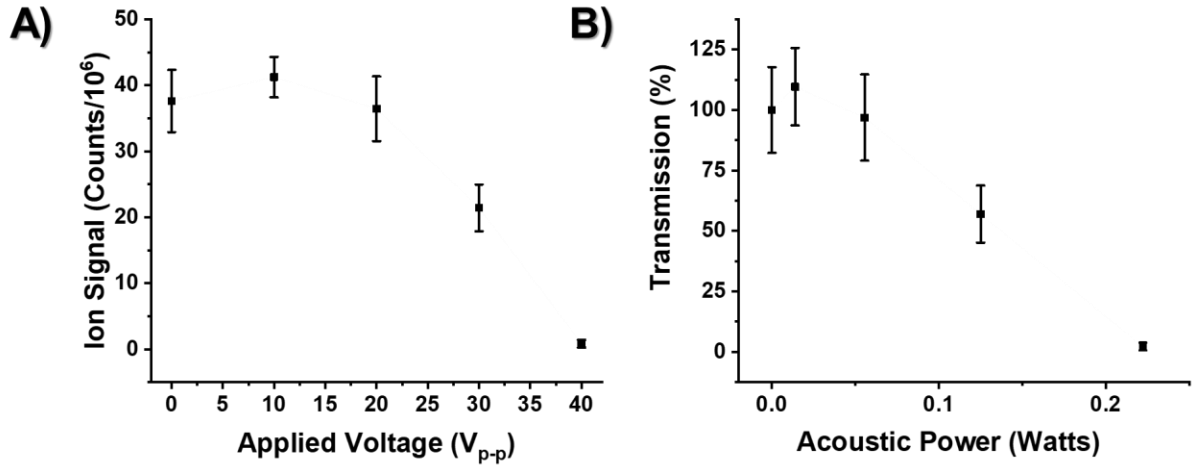

Figure 5. A) Total ion signal transmitting through the acoustic gate as a function of ultrasonic speaker voltage. B) Transmission through the gate as a function of theoretical acoustic power in the antinode. Acoustic power was calculated with the applied voltage and characteristic impedance (900 Ω) of the transducer at resonant frequency as described in equation 2. Source conditions were a flow rate of 0.5 L min^{-1} and a discharge current of 15 mA. A mass spectrometer was used as the detector.

where $P_{acoustic}$ is the average acoustic power, V_{peak} is the peak voltage of the sine wave, and R is the impedance of the transducer. Overall, a greater degree of ion blockage was observed at larger acoustic powers. There was a slight inconsistency in this trend between an acoustic power of 0 and 0.01 W, where ion signal increased in the presence of a weak acoustic field, but this is not statistically significant ($p = 0.5$). Although an exact explanation for this discrepancy is unknown, it could be attributed to changes in the vacuum environment around the mass spectrometer inlet caused by the low powered acoustic field. Ion leakage decreased linearly between 0.06 W and 0.2 W, with the lowest transmission of 2.2 ± 1.6% (*cf.* **Figure 5b**). Alignment of source, antinode, and detector must be carefully controlled, so that the ion beam impinges upon the gate where the acoustic power is strongest to yield maximum deflection.

Unsurprisingly, the velocity of the ion beam v, increased by a higher gas flow rate ($v = Q/A$ with Q being the flow rate and A the orifice area) or a repelling electric field (v = KE with K …), had a strong relationship to the leakage of the AIM ion gate. Generally, transmission through an acoustic ion gate increased monotonically with the average linear velocity of the gas (*cf.* **Figure 6a**). There was a small discrepancy between the two slowest velocities, 3.8 and 6.1 m s^{-1}, that we attribute to the gathering of slow-

moving ions by the mass spectrometer after deflection occurs. Importantly, the differences in measured transmission between these flow rates was not statistically significant (p value = 0.1).

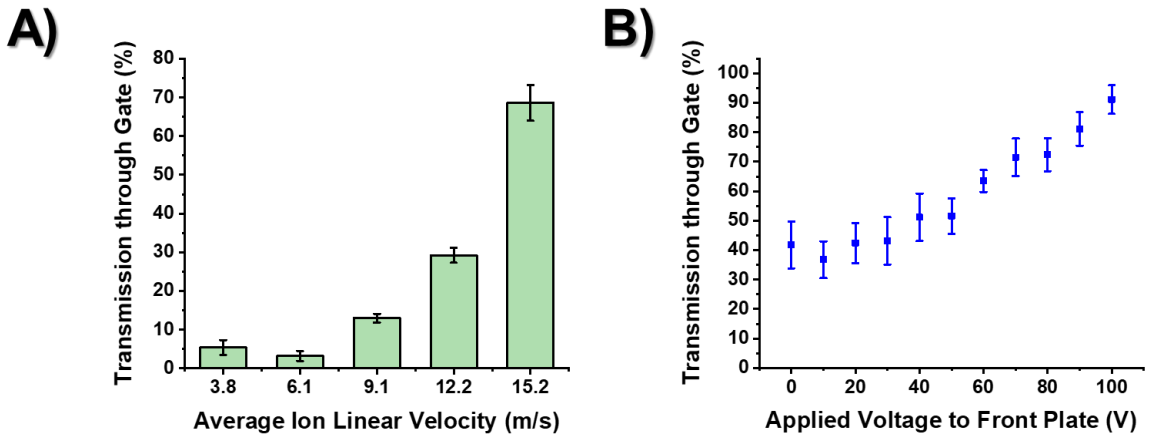

Figure 6: A) Transmission of ions through an antinode into a mass spectrometer depends on the linear velocity of the ion beam. The source was operated at helium flow rates 0.25, 0.4, 0.6, 0.8, and 1.0 L min^{-1}. with a discharge current of 15 mA. B) Transmission through an antinode was studied based on potential difference between the source and MS inlet. The distance between the biased source outlet and mass spectrometer inlet was *ca.* 20 mm. The source was operated with at a flow rate of 0.75 L min^{-1}, and a discharge current of 10 mA.

Similar to the gas flow rate, the presence of a DC electric field between the source and MS inlet in the direction of ion motion will also impact the kinetic properties of the ion beam. By biasing the exit capillary of the FAPA between 0 and 100 V_{DC}, the ions were pushed toward the mass spectrometer at higher velocities based on the potential difference. The inlet of the mass spectrometer is effectively at ground potential and does not contribute significantly to the ion velocity. As the ion beam was composed of many ion species with different mobilities, an accurate estimation of average ion velocity $\langle v_i \rangle$, was not possible. Nonetheless, under ambient conditions, the ion motion under external electric field is governed by the Nernst-Einstein relation, resulting in a linear velocity response of the ions under the presence of a static electric field. Here, the average linear velocity was estimated by referencing the experimentally determined transmission at different gas flow rates. It was found that lower potential differences (*i.e.* below 30 V) had average linear velocities of *ca.* 14 m s^{-1}, and little change in ion leakage through the closed gate was observed. Between a potential difference of 30 V and 100 V, the closed-gate transmission increased linearly

with rising field strengths (*cf.* **Figure 6b**). At the greatest potential difference of 100 V, the ions had an estimated average linear velocity of *ca.* 16 m s^{-1} and more than 90% leakage was observed. It can be summarized that electrostatic acceleration of ions to a higher average velocity led to a similar effect as observed in the case of ion velocity determined by flow rate.

While the exact mechanism responsible for ion deflection is still unclear, it is likely that the increased transmission observed at higher ion velocities was a result of fewer ions being deflected. Previous work has shown that the deflection of *ca.* 5-µm particles with a standing acoustic field is less effective at high flow rates.[34,35] It is important to note that the particles in these studies are significantly larger than gas-phase ions, and often in solution during acoustic interactions. Velocity is also a key component in the deflection of charged particles in electric and magnetic fields, where fast-moving ions are less impacted by field forces.[1] Likewise for AIM, it is apparent that momentum, collision cross-section and/or kinetic energy are critical for determining whether an ion will overcome the acoustic energy barrier (i.e. antinode). Clearly the degree of ion blockage by the acoustic ion gate can be altered through control of average ion velocity.

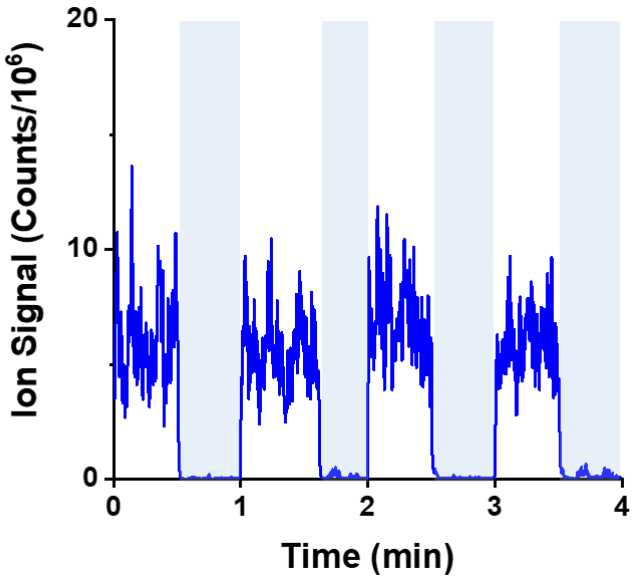

Figure 7: Total ion chronogram at optimized conditions (flow rate: 0.5 LPM, discharge current: 15 mA, 0V applied bias) with one ion gate. Shaded regions indicate the gate is closed. Resolving power was set to 17,500 and injection time to 50 ms to maximize spectral acquisition rate (13.3 Hz).

Following this line of thinking, the acoustic ion gate was most effective when average ion velocity was minimized by operating the ionization source without an external electric field at a helium flow rate of 0.5 L min^{-1}. At these conditions, the gate leakage as observed with MS was 1.8 ± 1.3% (*cf.* **Figure 7**). Unlike a BNG, which can obstruct ion passage by up to 20% even when the gate is open,[11] the acoustic ion gate allows all ions through when in the open state. Not only does this provide 100% ion throughput in the open state, it also eliminates any potential contamination due to interactions with a physical surface. Additionally, theoretically the gate can be opened or closed within tens of microseconds, which is on par with gate opening times required for IMS, between 50 and 200 μs (*cf.* **Figure 7**).[9] The standing wave is formed upon superposition of the two opposing wavefronts, so the turn-on time is estimated to be 23 μs, as that is the time it takes a *ca.* 40 kHz wave to travel half of the distance between the ultrasonic speakers, which are spaced 16 mm apart.[36] This duration is less than the scan time of the mass spectrometer (*ca.* 75 ms) when operated at a resolving power of 17,500 as observed in **Figure 7** and would suffice as a temporal gate in most linear drift tube IMS instruments. As such, the gate was established within one mass-spectral scan and finer detail could not be observed.

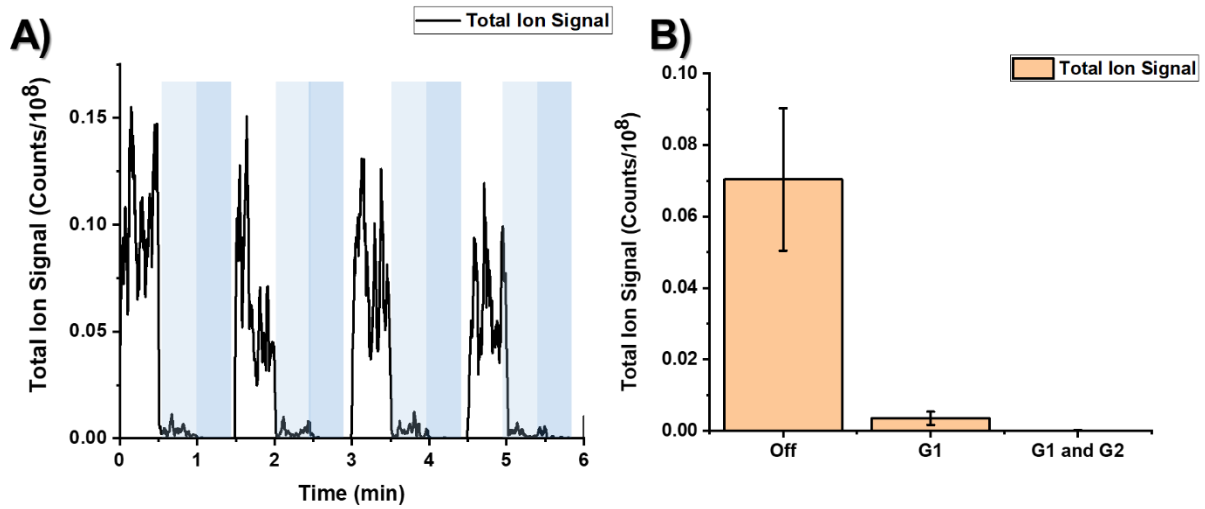

Figure 8: A) Total ion chronogram of single and dual ion gating. The lighter blue shading indicates one gate is present, while the darker shading indicates two gates are present. The source conditions were a flow rate of 0.5 L min^{-1} and a discharge current of 15 mA. B) Average ion signals are given for when zero, one, or two acoustic gates are present in the ion beam path.

The wide variety of transducers and easily controlled field properties (*e.g.* frequency, power) make acoustic gates ideal for customization and tailored design. For example, it is possible to add a second gate in sequence without much additional size, weight, and power. In these experiments, the acoustic ion gates were powered from the same function generator, but on different channels to enable independent operation. Additionally, the acoustic fields were separated by *ca.* 1 cm to accommodate the transducer casing and holder. The addition of a second gate required the ionization source to be moved back an additional 16 mm to accommodate the width of the additional transducers. Otherwise, ionization source parameters were the same as in single gate experiments and the transducers were driven at 37.8 kHz, 40 $V_{p\text{-}p}$. With a second gate, leakage declined to 0.2 ± 0.1% for a flow rate of 0.5 L min^{-1} (*cf.* **Figure 8**), a 10-fold improvement over a single acoustic gate. Additionally, the presence of two gates decreased transmission for ions at higher flow rates, indicating the adaptability of acoustic gates for a variety of potential experimental conditions. For a flow rate of 1 L min^{-1}, the transmission through two gates is 3.8 ± 1.1% (*cf.* **SI 4**). Non-zero transmission for a single ion gate can be attributed to ions penetrating through the antinode due to their unique speed or alignment with the acoustic field. Ions within the laminar flow of the bulk beam may move

faster or slower than the average linear velocity of the beam and may be aligned with the area between the node and antinode rather than with the antinode itself.[37] One possible explanation for this behavior is that ions which were not deflected by the first gate could be deflected by the second. The use of a second gate decreased leakage to be comparable to BNGs and TPGs, which are capable of blocking more than 99% of ions.

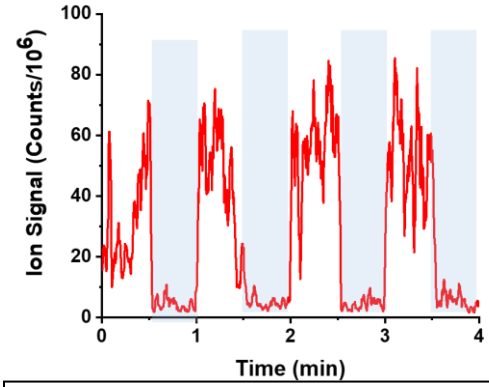

Figure 9: Extracted ion chronogram for aniline (*m/z* 94.0655), where shaded regions indicate the gate is closed.

Lastly, acoustic gating was applied to a small molecular compound to show efficacy for potential MS and IMS analytes. Aniline is a common commodity chemical and could be of interest due to its presence in many organic syntheses. Here, the ion beam was doped by passing nitrogen gas (0.06 L min^{-1}) over a vial with aniline and introducing the resulting gas stream to the FAPA ion beam. The protonated molecular ion of aniline was observed at *m/z* 94.0655 and exhibited transmission of 10.9 ± 4.6% through the ion gate, which was operated at 37.8 kHz and 40 V_{p-p} (*cf.* **Figure 9**). It is important to note that the introduction of aniline was done in the open-lab atmosphere, possibly contributing to the variability in signal due to ambient air currents. Disruptions to the exit flow of aniline from the vial by drafts led to inconsistent introduction of aniline to the FAPA beam and the reagent ions, and therefore caused inconsistent ionization efficiencies. However, it is still clear that the acoustic gate was able to block aniline post ionization from entering the mass spectrometer.

An AIM gate is comparable in basic function to an electrostatic gate, in terms of gating time and blockage efficiency. However, an acoustic gate has clear advantages in terms of ease of construction and support electronics. Traditional BNGs need to be biased above the drift potential in IMS instruments to reach the onset voltage for gating and often require custom-built electronics.[11,38] In contrast, an acoustic gate blocked more than 97% of ions without the use of electric fields in the gating region. The transducers for acoustic gating are operated at low driving voltages using commercially available power supplies. Additionally, the speaker components of the acoustic field are inexpensive (below $1.00 USD each) and easily replaceable. No electric shielding or isolation is necessary between acoustic gates either, as there are no electric fields present in the standing acoustic field region. Overall, the qualities of an acoustic-based ion gate make them user-friendly and inexpensive in comparison to traditional electrostatic lenses when implemented in ion-spectroscopy instrumentation.

CONCLUSIONS

This work demonstrates the possibility for a low-power, acoustic-based ion gate. Unlike several popular ion gates, such as a Bradbury-Nielsen or Tyndall-Powell gate, an AIM gate is 100% transparent, which reduces the possibility of analyte ion loss or sample contamination due to physical collisions with the gate mesh. Because there are no electric fields in the gating region, this gate does not impact sensitivity due to the presence of a depletion region. Additionally, it is constructed and powered with commercial electronics, eliminating the need for custom-built components. The acoustic ion gate is capable of operating at high pressures, such as for IMS analysis, and can interface with atmospheric pressure inlets, such as on a mass spectrometer. While more work is required to understand the underlying causes of gating behavior, we present the first steps towards developing new techniques for ion manipulation at atmospheric pressure without the use of electrostatic forces.

ACKNOWLEDGEMENTS

We thank and acknowledge Prof. R. Graham Cooks at Purdue University for loan of the IonCCD used in these experiments. We also acknowledge the Slezak fellowship and undergraduate student research fund granted by the Department of Chemistry and Chemical Biology at Rensselaer Polytechnic Institute for financial support of JLD.

REFERENCES

(1) Gross, J. H. *Mass Spectrometry*; Springer International Publishing: Cham, 2017. https://doi.org/10.1007/978-3-319-54398-7.

(2) Eiceman, G. A.; Karpas, Z. *Ion Mobility Spectrometry*, 2nd ed.; CRC Press: Boca Raton, FL.

(3) Drees, C.; Höving, S.; Vautz, W.; Franzke, J.; Brandt, S. 3D-Printing of a Complete Modular Ion Mobility Spectrometer. *Mater. Today* **2021**, *44*, 58–68. https://doi.org/10.1016/j.mattod.2020.10.033.

(4) Ni, K.; Guo, J.; Ou, G.; Zhang, X.; Yu, Q.; Qian, X.; Wang, X. Study of Ion Transmission for a Linear Mode Bradbury–Nielsen Gate in Ion Mobility Spectrometer. *Int. J. Mass Spectrom.* **2015**, *379*, 75–79. https://doi.org/10.1016/j.ijms.2014.12.012.

(5) Chen, C.; Tabrizchi, M.; Li, H. Ion Gating in Ion Mobility Spectrometry: Principles and Advances. *TrAC Trends Anal. Chem.* **2020**, *133*, 116100. https://doi.org/10.1016/j.trac.2020.116100.

(6) *SLIM Tricks: Tools, Concepts, and Strategies for the Development of Planar Ion Guides*. https://doi.org/10.1021/jasms.3c00163.

(7) Twyman, R. M. MASS SPECTROMETRY | Multidimensional. In *Encyclopedia of Analytical Science (Second Edition)*; Worsfold, P., Townshend, A., Poole, C., Eds.; Elsevier: Oxford, 2005; pp 430–438. https://doi.org/10.1016/B0-12-369397-7/00354-X.

(8) Puton, J.; Knap, A.; Siodłowski, B. Modelling of Penetration of Ions through a Shutter Grid in Ion Mobility Spectrometers. *Sens. Actuators B Chem.* **2008**, *135* (1), 116–121. https://doi.org/10.1016/j.snb.2008.08.011.

(9) Garcia, L.; Saba, C.; Manocchio, G.; Anderson, G. A.; Davis, E.; Clowers, B. H. An Open Source Ion Gate Pulser for Ion Mobility Spectrometry. *Int. J. Ion Mobil. Spectrom.* **2017**, *20* (3), 87–93. https://doi.org/10.1007/s12127-017-0223-x.

(10) Bradbury, N. E.; Nielsen, R. A. Absolute Values of the Electron Mobility in Hydrogen. *Phys. Rev.* **1936**, *49* (5), 388–393. https://doi.org/10.1103/PhysRev.49.388.

(11) Yoon, O. K.; Zuleta, I. A.; Robbins, M. D.; Barbula, G. K.; Zare, R. N. Simple Template-Based Method to Produce Bradbury-Nielsen Gates. *J. Am. Soc. Mass Spectrom.* **2007**, *18* (11), 1901–1908. https://doi.org/10.1016/j.jasms.2007.07.030.

(12) Zuleta, I. A.; Barbula, G. K.; Robbins, M. D.; Yoon, O. K.; Zare, R. N. Micromachined Bradbury−Nielsen Gates. *Anal. Chem.* **2007**, *79* (23), 9160–9165. https://doi.org/10.1021/ac071581e.

(13) Kirk, A. T.; Zimmermann, S. Bradbury-Nielsen vs. Field Switching Shutters for High Resolution Drift Tube Ion Mobility Spectrometers. *Int. J. Ion Mobil. Spectrom.* **2014**, *17* (3), 131–137. https://doi.org/10.1007/s12127-014-0153-9.

(14) Chen, C.; Chen, H.; Li, H. Pushing the Resolving Power of Tyndall–Powell Gate Ion Mobility Spectrometry over 100 with No Sensitivity Loss for Multiple Ion Species. *Anal. Chem.* **2017**, *89* (24), 13398–13404. https://doi.org/10.1021/acs.analchem.7b03629.

(15) Tyndall, A. M.; Powell, C. F.; Chattock, A. P. The Mobility of Ions in Pure Gases. *Proc. R. Soc. Lond. Ser. Contain. Pap. Math. Phys. Character* **1997**, *129* (809), 162–180. https://doi.org/10.1098/rspa.1930.0149.

(16) Chen, H.; Chen, C.; Li, M.; Wang, W.; Jiang, D.; Li, H. Achieving High Gating Performance for Ion Mobility Spectrometry by Manipulating Ion Swarm Spatiotemporal Behaviors in the Vicinity of Ion Shutter. *Anal. Chim. Acta* **2019**, *1052*, 96–104. https://doi.org/10.1016/j.aca.2018.11.045.

(17) Yang, Q.; Xu, Y.; Pan, M.; Jiang, D.; Wang, Z.; Wang, W.; Shi, X.; Chen, C.; Li, H. Enhancing the Performance of Tyndall–Powell Gate Ion Mobility Spectrometry by Combining Ion Enrichment, Discrimination Reduction, and Temporal Compression into a Single Gating Process. *Anal. Chem.* **2024**. https://doi.org/10.1021/acs.analchem.4c00582.

(18) Kirk, A. T.; Kueddelsmann, M. J.; Bohnhorst, A.; Lippmann, M.; Zimmermann, S. Improving Ion Mobility Spectrometer Sensitivity through the Extended Field Switching Ion Shutter. *Anal. Chem.* **2020**, *92* (7), 4838–4847. https://doi.org/10.1021/acs.analchem.9b04259.

(19) Yi You; Danischewski, J.; Molnar, B. T.; Riedel, J.; Shelley, J. T. Manipulation of Gaseous Ions with Acoustic Fields at Atmospheric Pressure. *J. Am. Chem. Soc.* **2024**, In submission.

(20) Marzo, A.; Barnes, A.; Drinkwater, B. W. TinyLev: A Multi-Emitter Single-Axis Acoustic Levitator. *Rev. Sci. Instrum.* **2017**, *88* (8), 085105. https://doi.org/10.1063/1.4989995.

(21) Zhao, S.; Wallaschek, J. A Standing Wave Acoustic Levitation System for Large Planar Objects. *Arch. Appl. Mech.* **2011**, *81* (2), 123–139. https://doi.org/10.1007/s00419-009-0401-3.

(22) Andrade, M. A. B.; Pérez, N.; Adamowski, J. C. Review of Progress in Acoustic Levitation. *Braz. J. Phys.* **2018**, *48* (2), 190–213. https://doi.org/10.1007/s13538-017-0552-6.

(23) Jackson, D. P.; Chang, M.-H. Acoustic Levitation and the Acoustic Radiation Force. *Am. J. Phys.* **2021**, *89* (4), 383–392. https://doi.org/10.1119/10.0002764.

(24) Andrade, F. J.; Shelley, J. T.; Wetzel, W. C.; Webb, M. R.; Gamez, G.; Ray, S. J.; Hieftje, G. M. Atmospheric Pressure Chemical Ionization Source. 1. Ionization of Compounds in the Gas Phase. *Anal. Chem.* **2008**, *80* (8), 2646–2653. https://doi.org/10.1021/ac800156y.

(25) Andrade, F. J.; Shelley, J. T.; Wetzel, W. C.; Webb, M. R.; Gamez, G.; Ray, S. J.; Hieftje, G. M. Atmospheric Pressure Chemical Ionization Source. 2. Desorption−Ionization for the Direct Analysis of Solid Compounds. *Anal. Chem.* **2008**, *80* (8), 2654–2663. https://doi.org/10.1021/ac800210s.

(26) Shelley, J. T.; Chan, G. C.-Y.; Hieftje, G. M. Understanding the Flowing Atmospheric-Pressure Afterglow (FAPA) Ambient Ionization Source through Optical Means. *J. Am. Soc. Mass Spectrom.* **2012**, *23* (2), 407–417. https://doi.org/10.1007/s13361-011-0292-8.

(27) Pfeuffer, K. P.; Shelley, J. T.; Ray, S. J.; Hieftje, G. M. Visualization of Mass Transport and Heat Transfer in the FAPA Ambient Ionization Source. *J. Anal. At. Spectrom.* **2013**, *28* (3), 379. https://doi.org/10.1039/c3ja30353e.

(28) Pfeuffer, K. P.; Ray, S. J.; Hieftje, G. M. Measurement and Visualization of Mass Transport for the Flowing Atmospheric Pressure Afterglow (FAPA) Ambient Mass-Spectrometry Source. *J. Am. Soc. Mass Spectrom.* **2014**, *25* (5), 800–808. https://doi.org/10.1007/s13361-014-0843-x.

(29) Hadjar, O.; Johnson, G.; Laskin, J.; Kibelka, G.; Shill, S.; Kuhn, K.; Cameron, C.; Kassan, S. IonCCD™ for Direct Position-Sensitive Charged-Particle Detection: From Electrons and keV Ions to Hyperthermal Biomolecular Ions. *J. Am. Soc. Mass Spectrom.* **2011**, *22* (4), 612–623. https://doi.org/10.1007/s13361-010-0067-7.

(30) 40T-12, 40R-12 Datasheet.

(31) Hadjar, O.; Fowler, W. K.; Kibelka, G.; Schnute, W. C. Preliminary Demonstration of an IonCCD as an Alternative Pixelated Anode for Direct MCP Readout in a Compact MS-Based Detector. *J. Am. Soc. Mass Spectrom.* **2012**, *23* (2), 418–424. https://doi.org/10.1007/s13361-011-0286-6.

(32) Skoblin, M.; Chudinov, A.; Soulimenkov, I.; Brusov, V.; Kozlovskiy, V. Gas Flow in the Capillary of the Atmosphere-to-Vacuum Interface of Mass Spectrometers. *J. Am. Soc. Mass Spectrom.* **2017**, *28* (10), 2132–2142. https://doi.org/10.1007/s13361-017-1743-7.

(33) Xia, C.; Mernie, E.; Zaia, J.; Costello, C. E.; Lin, C. Accurate Collisional Cross Section Measurement by Multipass Cyclic Ion Mobility Spectrometry. *Anal. Chem.* **2024**. https://doi.org/10.1021/acs.analchem.4c01758.

(34) Kalb, D. M.; Fencl, F. A.; Woods, T. A.; Swanson, A.; Maestas, G. C.; Juárez, J. J.; Edwards, B. S.; Shreve, A. P.; Graves, S. W. Line-Focused Optical Excitation of Parallel Acoustic Focused Sample Streams for High Volumetric and Analytical Rate Flow Cytometry. *Anal. Chem.* **2017**, *89* (18), 9967–9975. https://doi.org/10.1021/acs.analchem.7b02319.

(35) Wrede, P.; Aghakhani, A.; Bozuyuk, U.; Yildiz, E.; Sitti, M. Acoustic Trapping and Manipulation of Hollow Microparticles under Fluid Flow Using a Single-Lens Focused Ultrasound Transducer. *ACS Appl. Mater. Interfaces* **2023**, *15* (45), 52224–52236. https://doi.org/10.1021/acsami.3c11656.

(36) Martin, R.; Neary, E.; Rinaldo, J.; Woodman, O. *Introductory Physics: Building Models to Describe Our World*; 2021.

(37) Fowles, G.; Boyes, W. H. Chapter 6 - Measurement of Flow. In *Instrumentation Reference Book (Fourth Edition)*; Boyes, W., Ed.; Butterworth-Heinemann: Boston, 2010; pp 31–68. https://doi.org/10.1016/B978-0-7506-8308-1.00006-1.

(38) Tabrizchi, M.; Shamlouei, H. R. Relative Transmission of Different Ions through Shutter Grid. *Int. J. Mass Spectrom.* **2010**, *291* (1), 67–72. https://doi.org/10.1016/j.ijms.2010.01.011.